Int. J. Heat Mass Transfer. Vol. 26, No. 10, pp. 1557–1570, 1983
Printed in Great Britain

0017-9310/83 $3.00 + 0.00
Pergamon Press Ltd.

SECOND-ORDER BOUNDARY-LAYER FLOW PAST SHARP CONES

M. N. MATHUR†

Institut für Experimentelle Strömungsmechanik, Deutsche Forschungs- und Versuchsanstalt für Luft- und Raumfahrt e.V., Aerodynamische Versuchsanstalt, Bunsenstraße 10, D-3400 Göttingen, F.R.G.

(*Received* 14 *May* 1982 *and in revised form* 4 *October* 1982)

Abstract—Second-order boundary-layer effects of displacement thickness, transverse curvature, wall slip and temperature jump have been investigated in detail for flow past sharp cones of 5°, 10° and 15° semi-vertex angles. Similar solutions of the non-dimensional first- and second-order boundary-layer equations exist and numerical solutions of the resulting systems of ordinary-differential equations have been obtained using the finite-difference technique with variable step size. The second-order effects have been computed for different values of Mach number, wall temperature, and injection parameter. Some of the first-order results for wall heat transfer have been compared with the available experimental results at DFVLR.

NOMENCLATURE

a_1 constant appearing in the expression for wall slip condition, equations (4)
c_1 constant appearing in the temperature jump condition, equations (4)
c_f skin-friction coefficient
c_Q heat-transfer coefficient
CH_1 first-order boundary-layer rate of heat transfer at the surface
E constant in viscosity law, equation (5)
F function appearing in the first-order radial velocity component
G function defining the quantity $\bar{V}_1$, in the first-order boundary-layer flow
G_w value of G on cone surface
H first-order boundary-layer temperature distribution function
H_w value of H on cone surface
k thermal conductivity
L slant cone length
M the number of sub-divisions of the boundary-layer domain
M_∞ free-stream Mach number
p non-dimensional pressure
P_1, P_2 functions in the outer expansion for p
p_1, p_2 functions in the inner expansion for p
p_w value of p on cone surface
P_e inviscid first-order pressure on cone surface
r non-dimensional radial coordinate
R ratio of successive variable step sizes
R_e inviscid first-order density on cone surface
$R_1, R_2 \ldots$ functions in the outer expansion for ρ
T non-dimensional temperature
$T_1, T_2 \ldots$ functions in the outer expansion for T
T_w value of T on cone surface
T_∞ free-stream temperature
$t_1, t_2 \ldots$ functions in the inner expansion for T
$\bar{t}_1, \bar{t}_2 \ldots$ functions in the expressions for $t_1, t_2 \ldots$
T_e inviscid first-order temperature on cone surface
u non-dimensional velocity in r-direction
$U_1, U_2 \ldots$ functions in the outer expansion for u
$u_1, u_2 \ldots$ functions in the inner expansion for u
$\bar{u}_1, \bar{u}_2 \ldots$ functions in the expressions for $u_1, u_2 \ldots$
U_e first-order inviscid velocity component in r-direction on cone surface
U_∞ free-stream velocity
U function in the expression for $\bar{u}_2$
v non-dimensional velocity component in θ-direction
$V_1, V_2 \ldots$ functions in the outer expansion for v
$v_1, v_2 \ldots$ functions in the inner expansion for v
$\bar{v}_1, \bar{v}_2 \ldots$ functions in the expressions for $v_1, v_2 \ldots$
$\bar{V}_1, \bar{V}_2 \ldots$ functions defining the quantities

$$\bar{\rho}_1\left(\frac{\eta\bar{u}_1}{2}+\bar{v}_1\right) \text{ and } \bar{\rho}_1\left(\frac{\eta\bar{u}_2}{2}+\bar{v}_2\right)$$

V function in the expression for $\bar{v}_2$
$v_w(r)$ suction/injection velocity on cone surface
W function in the expression for $\bar{t}_2/\bar{t}_1$
Z quantity appearing in the expression for $\bar{\eta}$, equation (43)

Greek symbols

α cone semi-vertex angle
γ ratio of constant specific heats of the fluid
ε perturbation parameter, defined by equation (2)
η similarity variable
$\bar{\eta}$ the coordinate defined by $\int_0^\eta \bar{\rho}_1(s)\,ds$
θ angle between the radius vector and the cone axis
Θ stretched coordinate in θ-direction
κ^* value of the product $R_e T_e$
μ viscosity
ξ transformed coordinate in r-direction

† On leave from the Department of Mathematics, Indian Institute of Technology, Powai, Bombay 400076, India.

ρ density
$\rho_1, \rho_2 \ldots$ functions in the inner expansion for ρ
$\bar{\rho}_1, \bar{\rho}_2 \ldots$ functions in the expressions for $\rho_1, \rho_2 \ldots$
σ Prandtl number

1. INTRODUCTION

THE FLOW around a pointed cone is one of the most important in the study of aerodynamics of revolving bodies and has great practical value. Hantzsche and Wendt [1] have transformed the laminar boundary-layer equations for the supersonic flow past cones to the equations for the flow past a flat plate and have established relationships for boundary-layer thickness, skin-friction coefficient and the rate of heat transfer for the flows past cones and flat plates. Krasnov [2] calculated skin friction and heat transfer for the laminar boundary-layer flow past cones using the integral form of the governing equations. Very recently Krasil'schikov and Nosov [3] have studied experimentally some aerodynamic properties of cones in viscous supersonic flow. In all these studies, the effects of inviscid–viscous flow interaction, transverse curvature, wall slip and temperature jump at the surface have not been taken into account. These effects assume significance at high Mach numbers and in the presence of blowing.

It is well known that the classical boundary-layer theory is valid only when:

(a) the boundary-layer thickness is small in comparison with a characteristic curvature dimension of the body surface, and
(b) the rate of growth of the boundary-layer thickness is small.

Under extreme conditions of fluid motion, particularly in very high-speed flight at high altitude, the boundary layer near a surface can become sufficiently thick to materially affect the external flow. In turn, this influences the forces and heat transfer at the wall. At the same time and to the same order, roughly speaking, other assumptions of the classical boundary-layer theory begin to break down. Under these circumstances it becomes necessary to take into account the effects due to the boundary layer itself (displacement thickness effect), non-uniformities in the external stream, curvature of the surface, wall slip and temperature jump at the surface. The classical boundary-layer theory has been extended to deal with these effects. This extension of the classical boundary-layer theory has been termed higher-order boundary-layer theory, an excellent critical review of which was given by Van Dyke [4]. The method of matched asymptotic expansions is particularly useful in developing higher approximations to the boundary-layer theory and Van Dyke has worked out the second-order solutions for incompressible [5, 6] and compressible [7] flows. Higher-order boundary-layer theory has received considerable attention from many authors, and a comprehensive bibliography may be found in Van Dyke's review [4].

Some attempts have been made earlier to study the effects of displacement, curvature, slip and temperature jump in the boundary-layer flow past sharp cones.

Probstein and Elliott [8] studied, as a first-order effect, the transverse curvature effect in compressible axially-symmetric laminar boundary-layer flow and found that for cones and cylinders with zero pressure gradient the first-order correction to the Mangler formulation shows that the effect on both the skin-friction coefficient and heat-transfer rate can become appreciable when the ratio of the boundary-layer thickness to the body radius has a value which is less than or of the order of unity. At a constant value of this parameter, the transverse curvature and displacement effects are increased in magnitude when either the ratio of the wall to free-stream temperature or Mach number is increased. All other conditions being equal, for the same value of this parameter the skin-friction coefficient and heat transfer increase on the cylinder is greater than on the cone. Lewis *et al.* [9] have studied mass transfer and first-order boundary-layer effects on cones at supersonic and hypersonic conditions. They found that the total drag increases due to the effects of displacement, transverse curvature, slip, and temperature jump. Mass transfer at the cone surface resulted in drag reduction. Further, under certain conditions, the effects of velocity slip and temperature jump were found to be quite significant.

The present work deals with the detailed study of the laminar boundary-layer flow past circular cones of 5°, 10°, and 15° semi-vertex angles at high Mach numbers. We have employed the singular perturbation technique to derive the non-dimensional boundary-layer equations of the first- and second-order in a spherical polar coordinate system with axial symmetry. The first-order boundary-layer equations describe the Prandtl boundary-layer flow while the second-order boundary-layer equations deal with the effects of displacement thickness, transverse curvature, wall slip, and temperature jump at the surface. We have considered these effects for different values of the wall to stagnation temperature ratio. The effect of injection at the cone surface has also been investigated.

Due to the linearity of the second-order boundary-layer equations, it is possible to study each second-order effect individually and thus determine their relative importance. Tables [10, 11] have been used to calculate the first-order outer inviscid conical flow. The second-order inviscid flow equations have been used to obtain relationships among the surface values of the second-order flow variables. These quantities enter into the second-order boundary-layer equations.

Similar solutions of the first- and second-order boundary-layer equations are obtained and the resulting sets of ordinary differential equations have been solved numerically by finite-difference technique with variable step size. The results are presented graphically and in tabular form. Some of the results of the first-order boundary-layer flow are found to be in

good agreement with the available experimental results at DFVLR, AVA, Göttingen.

2. ANALYSIS

The equations of continuity, momentum, energy, and state are rendered dimensionless by using the characteristic length L (slant cone length), free-stream velocity U_∞, $\rho_\infty U_\infty^2$ (twice the stagnation pressure), U_∞^2/c_p, $\mu(U_\infty^2/c_p)$, respectively, for the radial distance r from the vertex of the cone, the velocity components u, v in r and θ directions, the pressure p, the temperature T and the viscosity μ. r and θ are the coordinates of a point in the flow-field in the spherical polar coordinate system with axial symmetry. c_p is the specific heat at constant pressure. An ideal gas is assumed. c_p and the Prandtl number $\sigma = \mu c_p/k$ are assumed constant. k is the thermal conductivity of the fluid.

The entire flow-field between the shock and the cone surface is divided into two regions:

(a) outer inviscid flow, and
(b) boundary layer close to the cone surface.

The coordinate θ in the boundary layer is stretched and the new coordinate Θ is defined by the relation

$$\Theta = (\theta - \alpha)/\varepsilon \tag{1}$$

where α is the semi-vertex angle of the cone. The singular perturbation parameter ε is given by

$$\varepsilon = [\mu(U_\infty^2/c_p)/\rho_\infty U_\infty L]^{1/2}. \tag{2}$$

The equation of state is

$$p = [(\gamma-1)/\gamma]\rho T. \tag{3}$$

We assume different perturbation series in the two regions for the flow variables u, v, p, ρ and T.

In addition to the equations of continuity, momentum, energy, and state, a suitable viscosity law is also assumed. The system of equations is to be solved under the following boundary conditions on the cone surface:

$$\begin{aligned} u &= (\varepsilon^2 a_1/p_w)\{[(\gamma-1)/\gamma]T_w\}^{1/2}\left(\frac{\mu}{r}\frac{\partial u}{\partial \theta}\right)_{\theta=\alpha}, \\ v &= \varepsilon v_w(r), \\ T &= T_w + (\varepsilon^2 c_1/p_w)\{[(\gamma-1)/\gamma]T_w\}^{1/2}\left(\frac{\mu}{r}\frac{\partial T}{\partial \theta}\right)_{\theta=\alpha}. \end{aligned} \tag{4}$$

In the above equations $\gamma = c_p/c_v$, a_1 and c_1 are constants given by Street [12]. Equations (4) account for the non-continuum effects of wall slip and temperature jump. The subscript w refers to the cone surface and $v_w(r)$ is the variable velocity on the cone surface in θ direction. $v_w > 0$ gives injection and $v_w < 0$ means suction. In the present work, we have assumed $v_w > 0$.

In addition to the conditions given by equations (4), we apply the usual Rankine–Hugoniot conditions at the shock.

It will be shown in the latter part of the analysis that the pressure in the boundary layer is independent of the coordinate Θ. In view of this it is permissible to assume

$$\rho\mu = \text{constant} = E, \tag{5}$$

for viscosity.

The constant E can be assumed to be an average constant in the boundary layer depending upon the constant wall temperature T_w and the constant temperature T_e at the edge of the first-order boundary-layer flow. Gersten *et al.* [13] have assumed $\rho\mu = \rho_w\mu_w = 1$ which amounts to regarding μ as a linear function of temperature if pressure across the boundary layer does not vary. Mitome and Yasuhara [14] have assumed

$$\frac{\rho\mu}{\rho_w\mu_w} = N$$

and have regarded N as an average constant in the boundary layer. N is taken to depend on the constant temperatures at the wall and the edge of the boundary layer. We have assumed the following relationship for E:

$$E = \kappa^* T_w^{1/2}\left(\frac{1+S_1}{T_w+S_1}\right)$$

where

$$\begin{aligned} \kappa^* &= R_e T_e, \\ S_1 &= 110.4^\circ\kappa/[(\gamma-1)M_\infty^2 T_\infty], \\ T_\infty &= T_s/[(\gamma-1)M_\infty^2 T_0]. \end{aligned}$$

T_∞ is the dimensional free-stream temperature, T_s is the dimensional stagnation temperature, T_0 is the dimensionless stagnation temperature, M_∞ is the free-stream Mach number, and R_e and T_e are the first-order outer inviscid flow density and temperature on the cone surface, respectively.

This choice of E implies that the linear viscosity law will give a better approximation to the more exact Sutherland formula in the temperature range close to the constant wall temperature [15].

In the following, we describe briefly the analysis in the two regions of the flow.

2.1. *Outer expansion*

In the outer inviscid flow region, we assume

$$u(r,\theta) = U_1(\theta) + \varepsilon U_2(r,\theta) + \ldots \tag{6}$$

with similar expansions for v, p, ρ and T.

On substituting these expansions in the non-dimensional equations of continuity, momentum, energy, and the equation of state (3) and equating the coefficients of ε^0 and ε^1, we obtain the first- and second-order equations for the flow in the outer region. The solution of the first-order conical flow is available in the form of tables [10, 11] and we have used these tables to compute the surface values

$$U_1(\theta=\alpha) = U_e, T_1(\theta=\alpha) = T_e, P_1(\theta=\alpha) = P_e,$$
$$R_1(\theta=\alpha) = R_e.$$

These quantities appear in the first- and second-order boundary-layer equations and the second-order outer flow quantities on the cone surface.

The second-order inviscid flow equations admit a solution of the form

$$U_2(r,\theta)=\frac{\bar{U}_2(\theta)}{r^{1/2}},\ V_2(r,\theta)=\frac{\bar{V}_2(\theta)}{r^{1/2}},$$

$$P_2(r,\theta)=\frac{\bar{P}_2(\theta)}{r^{1/2}}, \tag{7}$$

$$R_2(r,\theta)=\frac{\bar{R}_2(\theta)}{r^{1/2}},\ T_2(r,\theta)=\frac{\bar{T}_2(\theta)}{r^{1/2}}.$$

On substituting (7) in the second-order inviscid flow equations, we obtain a system of ordinary differential equations for $\bar{U}_2(\theta),\ldots,$ etc. This system of equations must be solved numerically to determine the complete solution of the second-order inviscid flow.

Our main interest here is to obtain the values of U_2, ..., etc. on the cone surface. This is done by writing the second-order inviscid flow equations on the cone surface and using the following first-order inviscid flow relations on the cone surface:

$$V_1(\theta=\alpha)=0,$$

(boundary condition for first-order flow)

$$\left(\frac{dV_1}{d\theta}+2U_1\right)_{\theta=\alpha}=0, \tag{8}$$

$$\left(\frac{dP_1}{d\theta}\right)_{\theta=\alpha}=0.$$

The second-order inviscid flow equations, when written on the cone surface, give the following relations:

$$\left(R_1U_1\frac{\partial U_2}{\partial r}\right)_{\theta=\alpha}=-\left(\frac{\partial P_2}{\partial r}\right)_{\theta=\alpha}$$

$$\left(R_1\frac{\partial T_2}{\partial r}\right)_{\theta=\alpha}=\left(\frac{\partial P_2}{\partial r}\right)_{\theta=\alpha} \tag{9}$$

$$P_2(r,\alpha)=\frac{\gamma-1}{\gamma}[R_2(r,\alpha)T_1(\alpha)+R_1(\alpha)T_2(r,\alpha)].$$

Making use of equations (7), we obtain from equation (9)

$$\bar{P}_2(\alpha)=-R_eU_e\bar{U}_2(\alpha)=R_e\bar{T}_2(\alpha)$$

$$=\frac{\gamma-1}{\gamma}[R_e\bar{T}_2(\alpha)+T_e\bar{R}_2(\alpha)]. \tag{10}$$

We have, from the first-order inviscid equation of state,

$$P_e=\frac{\gamma-1}{\gamma}R_eT_e.$$

From equation (10) we also have

$$\bar{T}_2(\alpha)=-U_e\bar{U}_2(\alpha). \tag{11}$$

It has been pointed out [9] that the displacement effect increases the pressure in the inviscid flow and this implies that $\bar{P}_2(\alpha)$ must be positive. In view of equations (10) and (11), $\bar{U}_2(\alpha)$ and $\bar{T}_2(\alpha)$, respectively, are negative and positive. The signs of $\bar{U}_2(\alpha)$ and $\bar{T}_2(\alpha)$ will determine the nature of the displacement effect on skin friction and heat transfer at the surface.

2.2. *Inner expansion*

The flow variables in the boundary-layer region are expressed in the following manner:

$$u(r,\theta)=u_1(r,\Theta)+\varepsilon u_2(r,\Theta)+\ldots, \tag{12}$$

with similar expansions for v, p, ρ and T. From equation (5), the viscosity μ can be expressed as

$$\mu=\frac{E}{\rho_1(r,\Theta)}\left[1-\varepsilon\frac{\rho_2(r,\Theta)}{\rho_1(r,\Theta)}+\ldots\right]. \tag{13}$$

The first- and second-order boundary-layer equations are obtained by substituting equations (12) and (13) into the full non-dimensional equations of continuity, momentum, energy, and state and equating the coefficients of ε^0 and ε^1. The corresponding boundary conditions at the surface are obtained in a similar manner from equations (4). The conditions at the boundary-layer edge are obtained by using the matching principle. We give below the complete sets of the first- and second-order boundary-layer equations along with the boundary and matching conditions.

First-order boundary-layer equations.

Continuity:

$$\frac{\partial}{\partial r}(\rho_1u_1)+\frac{2}{r}(\rho_1u_1)+\frac{1}{r}\frac{\partial}{\partial\Theta}(\rho_1v_1)=0. \tag{14}$$

Momentum:

$$\rho_1\left(u_1\frac{\partial u_1}{\partial r}+\frac{v_1}{r}\frac{\partial u_1}{\partial\Theta}\right)=\frac{E}{r^2}\frac{\partial}{\partial\Theta}\left(\frac{1}{\rho_1}\frac{\partial u_1}{\partial\Theta}\right). \tag{15}$$

Energy:

$$\rho_1\left(u_1\frac{\partial t_1}{\partial r}+\frac{v_1}{r}\frac{\partial t_1}{\partial\Theta}\right)=\frac{E}{r^2}\left[\frac{1}{\sigma}\frac{\partial}{\partial\Theta}\left(\frac{1}{\rho_1}\frac{\partial t_1}{\partial\Theta}\right)+\frac{1}{\rho_1}\left(\frac{\partial u_1}{\partial\Theta}\right)^2\right]. \tag{16}$$

Equation of state:

$$\rho_1t_1=(R_1T_1)_{\theta=\alpha}=R_eT_e=\text{constant}=\kappa^*. \tag{17}$$

Boundary conditions:

$$\Theta=0:\ u_1=0,\ v_1=v_w(r)=\frac{\tilde{V}_w}{r^{1/2}},$$

$$t_1=T_w=\text{constant}, \tag{18}$$

$$\Theta\to\infty:\ u_1\to u_e,\ t_1\to T_e.$$

$\tilde{V}_w$ is a constant quantity which is positive for injection and negative for suction at the cone surface. We have considered $\tilde{V}_w>0$ only because the second-order effects become increasingly significant at high Mach numbers and in the presence of blowing as stated in ref. [15].

Second-order boundary-layer equations.
Continuity:

$$\frac{\partial}{\partial r}(\rho_1 u_2+\rho_2 u_1)+\frac{2}{r}(\rho_1 u_2+\rho_2 u_1)$$
$$+\frac{1}{r}\frac{\partial}{\partial\Theta}(\rho_1 v_2+\rho_2 v_1)=-\frac{\rho_1 v_1\cot\alpha}{r}. \quad (19)$$
TC

Momentum:

$$\rho_1\left(u_1\frac{\partial u_2}{\partial r}+u_2\frac{\partial u_1}{\partial r}+\frac{v_1}{r}\frac{\partial u_2}{\partial\Theta}+\frac{v_2}{r}\frac{\partial u_1}{\partial\Theta}\right)$$
$$+\frac{E\rho_2}{r^2\rho_1}\frac{\partial}{\partial\Theta}\left(\frac{1}{\rho_1}\frac{\partial u_1}{\partial\Theta}\right)-\frac{E}{r^2}\frac{\partial}{\partial\Theta}\left(\frac{1}{\rho_1}\frac{\partial u_2}{\partial\Theta}-\frac{\rho_2}{\rho_1^2}\frac{\partial u_1}{\partial\Theta}\right)$$
$$=\left(R_1U_1\frac{\partial U_2}{\partial r}\right)_{\theta=\alpha}+\frac{E\cot\alpha}{r^2\rho_1}\frac{\partial u_1}{\partial\Theta} \quad (20)$$
D TC

Energy:

$$\rho_1\left(u_1\frac{\partial t_2}{\partial r}+u_2\frac{\partial t_1}{\partial r}+\frac{v_1}{r}\frac{\partial t_2}{\partial\Theta}+\frac{v_2}{r}\frac{\partial t_1}{\partial\Theta}\right)$$
$$+\frac{E\rho_2}{r^2\rho_1}\left[\frac{1}{\sigma}\frac{\partial}{\partial\Theta}\left(\frac{1}{\rho_1}\frac{\partial t_1}{\partial\Theta}\right)+\frac{2}{\rho_1}\left(\frac{\partial u_1}{\partial\Theta}\right)^2\right]$$
$$-\frac{E}{r^2\sigma}\frac{\partial}{\partial\Theta}\left(\frac{1}{\rho_1}\frac{\partial t_2}{\partial\Theta}-\frac{\rho_2}{\rho_1 2}\frac{\partial t_1}{\partial\Theta}\right)-\frac{2E}{r^2\rho_1}\frac{\partial u_1}{\partial\Theta}\frac{\partial u_2}{\partial\Theta}$$
$$=-u_1\left(R_1U_1\frac{\partial U_2}{\partial r}\right)_{\theta=\alpha}+\frac{E\cot\alpha}{r^2\sigma\rho_1}\frac{\partial t_1}{\partial\Theta}. \quad (21)$$
D TC

Equation of state:

$$\frac{\rho_2}{\rho_1}+\frac{t_2}{t_1}=\frac{1}{r^{1/2}}\left[\frac{\bar T_2(\alpha)}{T_e}+\frac{\bar R_2(\alpha)}{R_e}\right]. \quad (22)$$
D

Boundary conditions:

$$\Theta=0:\ u_2=\left[\frac{Ea_1(\gamma-1)^{1/2}t_1}{p_1\rho_1\gamma^{1/2}r}\frac{\partial u_1}{\partial\Theta}\right]_{\theta=0},$$
S
$$v_2=0,$$
$$t_2=\left[\frac{Ec_1(\gamma-1)^{1/2}t_1}{p_1\rho_1\gamma^{1/2}r}\frac{\partial t_1}{\partial\Theta}\right]_{\theta=0}, \quad (23)$$
TJ
$$\Theta\to\infty:\ u_2\to\frac{\bar U_2(\alpha)}{r^{1/2}},\ t_2\to\frac{\bar T_2(\alpha)}{r^{1/2}}.$$
D D

The first- and second-order momentum equations in Θ-direction lead to the fact that p_1 and p_2 remain invariant with respect to Θ and thus we obtain

$$p_1(r,\Theta)=P_1(\theta=\alpha)=P_e=\text{constant},$$
$$p_2(r,\Theta)=P_2(r,\theta=\alpha)=\frac{\bar P_2(\alpha)}{r^{1/2}}.$$

As a consequence of this relation, we have

$$\frac{\partial p_2}{\partial r}=\left(\frac{\partial P_2}{\partial r}\right)_{\theta=\alpha}=-\left(R_1U_1\frac{\partial U_2}{\partial r}\right)_{\theta=\alpha}$$

on using equation (9).

This confirms the statement made in writing equation (5) for viscosity. We have made use of the above expression for $\partial p_2/\partial r$ and equations (14)–(17) in writing equations (19)–(22). The terms on the RHS of equations (19)–(23) with the letters D, TC, S and TJ below them account, respectively for the effects of displacement, transverse curvature, wall slip, and temperature jump. Equations (19)–(23) are linear and this property has been used to study the contribution of each second-order effect separately. This has been done by splitting the functions u_2, v_2, ρ_2 and t_2 in the following manner:

$$u_2=u_2^{(D)}+u_2^{(TC)}+u_2^{(S)}+u_2^{(TJ)}$$

with similar expressions for other functions. This approach has been used by Van Dyke [7].

2.3. *Similar solutions of first- and second-order boundary-layer equations*

We transform (r,Θ) domain to (ξ,η) by applying the following transformations:

$$\xi=r,\quad \eta=\frac{r\Theta}{r^{1/2}}=r^{1/2}\Theta. \quad (24)$$

To further simplify the mathematical analysis, a new variable $\bar\eta$ is introduced. The relation between η and $\bar\eta$ is

$$\bar\eta=\int_0^\eta \rho_1(s)\,ds. \quad (25)$$

The dependent variables are written as

$$u_1=\bar u_1(\eta), v_1=\bar v_1(\eta)/\xi^{1/2}, t_1=\bar t_1(\eta),$$
$$\rho_1=\bar\rho_1(\eta), u_2=\bar u_2(\eta)/\xi^{1/2}, v_2=\bar v_2(\eta)/\xi,$$
$$t_2=\bar t_2(\eta)/\xi^{1/2}, \rho_2=\bar\rho_2(\eta)/\xi^{1/2}. \quad (26)$$

In terms of new variable $\bar\eta$, we write

$$\bar u_1=U_eF(\bar\eta), \bar V_1=U_eG(\bar\eta), \bar t_1=T_eH(\bar\eta)$$
$$\bar u_2=U_{2c}U(\bar\eta), \bar V_2=U_{2c}V(\bar\eta), \frac{\bar t_2}{\bar t_1}=\frac{T_{2c}}{T_e}W(\bar\eta), \quad (27)$$

where

$$\bar V_1=\bar\rho_1\left(\frac{\eta\bar u_1}{2}+\bar v_1\right)\quad\text{and}\quad \bar V_2=\bar\rho_1\left(\frac{\eta\bar u_2}{2}+\bar v_2\right).$$

U_{2c} and T_{2c} in equations (27) are constants and have the

following representations:

$U_{2c} = \bar{U}_2(\alpha)$, $T_{2c} = \bar{T}_2(\alpha)$ (for displacement effect)

and

$$U_{2c} = U_e, \quad T_{2c} = T_e \quad \text{(for other effects)}.$$

On substituting equations (24)–(27) in equations (14)–(23), we obtain the following systems of ordinary differential equations:

First-order boundary-layer similarity equations.† Continuity:

$$G' + \frac{3F}{2} = 0. \tag{28}$$

Momentum:

$$F'' - (U_e/E)GF' = 0. \tag{29}$$

Energy:

$$H'' - (\sigma U_e/E)GH' = -(\sigma U_e^2/T_e)(F')^2. \tag{30}$$

Equation of state:

$$\bar{\rho}_1 \bar{t}_1 = \kappa^*. \tag{31}$$

Boundary conditions:

$$\bar{\eta} = 0: F = 0, G = (\kappa^*/U_e)(\bar{V}_w/T_w) = G_w,$$
$$H = (T_w/T_e) = H_w, \quad \bar{\eta} \to \infty: F \to 1, H \to 1. \tag{32}$$

Second-order boundary-layer similarity equations. Continuity:

$$[(U_{2c}/U_e)V + (\bar{\rho}_2/\bar{\rho}_1)G]' + [(U_{2c}/U_e)U + (\bar{\rho}_2/\bar{\rho}_1)F] = -(\bar{v}_1/U_e)\cot\alpha. \tag{33}$$

TC

Momentum:

$$U_e U_{2c}[-\tfrac{1}{2}(FU) + GU' + VF'] + (\bar{\rho}_2/\bar{\rho}_1)EU_eF'' - E[U_{2c}U' - (\bar{\rho}_2/\bar{\rho}_1)U_eF']' = -\frac{R_eU_eU_2(\alpha)}{2\bar{\rho}_1} + \frac{EU_e\cot\alpha}{\bar{\rho}_1}F'. \tag{34}$$

D TC

Energy:

$$U_eT_{2c}[-\tfrac{1}{2}(FH)W + G(WH)'] + T_eU_{2c}VH' + (\bar{\rho}_2/\bar{\rho}_1)E\left[\frac{T_e}{\sigma}H'' + 2U_e^2(F')^2\right] - \frac{E}{\sigma}[T_{2c}(WH)' - (\bar{\rho}_2/\bar{\rho}_1)T_eH']' \tag{35}$$

$$-2EU_eU_{2c}F'U' = \frac{R_eU_e^2\bar{U}_2(\alpha)}{2\bar{\rho}_1}F + \frac{E(\cot\alpha)T_e}{\bar{\rho}_1\sigma}H'$$

D TC

† Primes denote differentiation with respect to $\bar{\eta}$.

Equation of state:

$$\frac{\bar{\rho}_2}{\bar{\rho}_1} + \frac{T_{2c}}{T_e}W = \frac{\bar{T}_2(\alpha)}{T_e} + \frac{\bar{R}_2(\alpha)}{R_e} = \frac{\bar{P}_2(\alpha)}{P_e} = \frac{R_e\bar{T}_2(\alpha)}{P_e}$$

D D D

$$= \frac{R_eT_e}{P_e}\frac{\bar{T}_2(\alpha)}{T_e} = \frac{\gamma}{\gamma-1}[\bar{T}_2(\alpha)/T_e]. \tag{36}$$

D D

Boundary conditions:

$\bar{\eta} = 0$:

$$U = (Ea_1/P_e)\left[\frac{(\gamma-1)T_w}{\gamma}\right]^{1/2}F'(0),$$

S

$$V = 0, \tag{37}$$

$$W = (Ec_1/P_e)\left[\frac{(\gamma-1)T_w}{\gamma}\right]^{1/2}[H'(0)/H_w],$$

TJ

$$\bar{\eta} \to \infty: U \to 1, W \to 1.$$

D D

In writing equation (36), we have made use of equations (10) and the relation $P_e = (\gamma-1)R_eT_e/\gamma$. $P_e = (\gamma-1)R_eT_e/\gamma$ is obtained from the first-order outer conical flow from the equation of state written on the cone surface.

Equation (36) gives

$$\frac{\bar{\rho}_2}{\bar{\rho}_1} = \frac{\bar{T}_2(\alpha)}{T_e}\left(\frac{\gamma}{\gamma-1} - W\right)$$

for the displacement effect and

$$\frac{\bar{\rho}_2}{\bar{\rho}_1} = -W$$

for the other second-order effects.

The boundary conditions for each second-order effect are obtained appropriately from equations (37).

2.4. *Skin-friction coefficient and wall heat-transfer coefficient*

The local shear stress at the wall $\tau_w(r)$ and the local wall heat-transfer coefficient $q_w(r)$, in terms of dimensional variables, have the following expressions:

$$\tau_w(r) = \left(\frac{\mu}{r}\frac{\partial\mu}{\partial\theta}\right)_{\theta=\alpha},$$

$$q_w(r) = -\left[\left(\frac{\mu c_p}{\sigma r}\frac{\partial T}{\partial\theta}\right) + \frac{\mu u}{r}\frac{\partial u}{\partial\theta}\right]_{\theta=\alpha}.$$

The second term in the expression for $q_w(r)$ is known as

the contribution due to sliding friction and accounts for the wall slip.

We define the dimensionless skin-friction coefficient c_f and the wall heat-transfer coefficient c_Q as

$$c_f = \frac{\tau_w}{\rho_\infty U_\infty^2} = \varepsilon c_f^{(1)} + \varepsilon^2 c_f^{(2)},$$
$$c_Q = \frac{q_w}{\rho_\infty U_\infty^3} = \varepsilon c_Q^{(1)} + \varepsilon^2 c_Q^{(2)}, \tag{38}$$

where

$$c_f^{(1)} = \frac{EU_e F'(0)}{r^{1/2}}, c_Q^{(1)} = -\frac{ET_e H'(0)}{r^{1/2}(\sigma)},$$
$$c_f^{(2)} = \frac{E}{r}[U_{2c}U'(0) - (\bar{\rho}_2/\bar{\rho}_1)_{\bar{\eta}=0} U_e F'(0)],$$
$$c_Q^{(2)} = -\frac{E}{r}\left\{\frac{T_{2c}}{\sigma}[W(0)H'(0) + H(0)W'(0)]\right. \tag{39}$$
$$- \frac{T_e}{\sigma}(\bar{\rho}_2/\bar{\rho}_1)_{\bar{\eta}=0} H'(0)$$
$$\left. + U_e U_{2c} F'(0) U(0)\right\}.$$

For the first-order boundary layer flow, we have computed $\varepsilon c_f^{(1)} r^{1/2}$ and CH_1, where

$$CH_1 = \frac{\varepsilon c_Q^{(1)}}{(T_0 - T_w)}.$$

The absolute value of CH_1 is the usual Stanton number, e.g. $St_1 = |CH_1|$.

To study the effects of displacement, transverse curvature, wall slip, and temperature jump at the surface, we have computed the following quantities:

$$\frac{c_f}{\varepsilon c_f^{(1)}} = 1 + \varepsilon c_f^{(2)}/c_f^{(1)} = 1 + \frac{\varepsilon}{r^{1/2}}\left[\frac{U_{2c}}{U_e}\frac{U'(0)}{F'(0)}\right.$$
$$\left. - (\bar{\rho}_2/\bar{\rho}_1)_{\bar{\eta}=0}\right] = 1 + \frac{\varepsilon}{r^{1/2}}(CF),$$
$$\frac{c_Q}{\varepsilon c_Q^{(1)}} = 1 + \varepsilon c_Q^{(2)}/c_Q^{(1)} = 1 + \frac{\varepsilon}{r^{1/2}}\left\{\frac{T_{2c}}{T_e}\{W(0)\right. \tag{40}$$
$$\left. + H(0)\frac{W'(0)}{H'(0)}\right] - (\bar{\rho}_2/\bar{\rho}_1)_{\bar{\eta}=0}$$
$$\left. + \frac{\sigma U_e U_{2c}}{T_e}\frac{F'(0)}{H'(0)}U(0)\right\} = 1 + \frac{\varepsilon}{r^{1/2}}(HQ).$$

CF and HQ are written below, separately, for each second-order effect.

Displacement:

$$CF = \frac{\bar{U}_2(\alpha)}{U_e}(CT), \quad CT = \frac{U'(0)}{F'(0)} + \frac{U_e^2}{T_e}\frac{\gamma}{\gamma - 1},$$
$$HQ = \frac{\bar{T}_2(\alpha)}{T_e}(CQ), \quad CQ = H(0)\frac{W'(0)}{H'(0)} - \frac{\gamma}{\gamma - 1}.$$

Transverse curvature:

$$CF = \frac{U'(0)}{F'(0)} = CT,$$
$$HQ = H(0)\frac{W'(0)}{H'(0)} = CQ. \tag{41}$$

Wall slip:

$$CF = \frac{U'(0)}{F'(0)} = CT,$$
$$HQ = H(0)\frac{W'(0)}{H'(0)} + \frac{\sigma U_e^2}{T_e}U(0)\frac{F'(0)}{H'(0)} = CQ.$$

Temperature jump:

$$CF = \frac{U'(0)}{F'(0)} + W(0) = CT,$$
$$HQ = 2W(0) + H(0)\frac{W'(0)}{H'(0)} = CQ.$$

3. COMPUTATIONAL PROCEDURE

In this section, we describe briefly the numerical method used for the solution of similarity equations obtained in Section 2.3. Equations (28)–(37) are solved by a finite-difference technique with variable step size. This technique has been discussed in detail by Blottner [16].

The boundary-layer region has been divided into a number of elementary regions by writing

$$\bar{\eta}_{j+1} = \bar{\eta}_j + \Delta\bar{\eta}_{j+1/2}, \quad j = 1, 2, 3, \ldots, M-1$$

where $\bar{\eta}_1 = 0$ gives the cone surface and $\bar{\eta}_M = \bar{\eta}_e$ the edge of the boundary layer.

This scheme can be interpreted in terms of a coordinate stretching approach. A new coordinate Z is introduced where a uniform interval ΔZ is used and is related to $\bar{\eta}$ by the relation

$$\bar{\eta}_j = \bar{\eta}(Z_j), \quad j = 1, 2, \ldots, M. \tag{42}$$

Equation (42), finally, can be written as

$$\bar{\eta}_j = \bar{\eta}_e(R^{Z_j/\Delta Z_0} - 1)/(R^{1/\Delta Z_0} - 1), \quad j = 1, 2, \ldots, M \tag{43}$$

where $Z_j = (j-1)\Delta Z$ and $Z_M = 1$. In equation (43), R is the ratio of two successive step sizes. R and ΔZ_0 are two parameters which can be chosen suitably to give the desired step-size spacing.

The expressions for the derivatives in terms of finite-differences are available in ref. [16].

We briefly outline the numerical method for the solution of the non-linear coupled equations (28)-(32). We decouple these equations and use an iterative process to solve each equation separately for a single dependent variable with suitable starting profiles. The iterative process is stopped when the difference between two successive iterates is less than 10^{-4}. For example, we solve equation (29) for F after replacing the derivatives in terms of finite-differences and solving the resulting system of linear algebraic equations using the Thomas algorithm [17]. This solution for F is used to

obtain G from the continuity equation, equation (28). Equation (30) is solved for the temperature distribution H. After this the same procedure is adopted to solve the equations (33)–(37) determining the functions for second-order boundary-layer flow.

The values of $F'(0), H'(0), U'(0)$ and $W'(0)$ occurring in equations (39)–(41) are calculated by using a special finite-difference expression which has been derived elsewhere [16].

With these expressions for the wall derivatives and the prescribed wall values of the functions F, H, U and W on the wall, we can calculate $c_f^{(1)}, c_Q^{(1)}, c_f^{(2)}, c_Q^{(2)}, CT$, and CQ with the help of equations (39) and (41). $c_f/\varepsilon c_f^{(1)}$ and $c_Q/\varepsilon c_Q^{(1)}$ then can be calculated from equations (40). This is to be noted that CF and HQ for the displacement effect can be computed numerically only when $\bar{U}_2(\alpha)$ and $\bar{T}_2(\alpha)$ are known from the second-order inviscid flow. We have already determined the signs of $\bar{U}_2(\alpha)$ and $\bar{T}_2(\alpha)$ which at least give the nature of the displacement effect on skin friction and wall heat transfer.

The data sets in Table 1 are those for which the computations have been carried out. Table 1 also shows the first-order inviscid flow quantities on the cone surface corresponding to the data sets. The values of the other parameters entering into calculations are given below:

$$M = 61, \bar{\eta}_e = 6, R = 1.0025, \Delta Z_0 = 0.1,$$

$$\gamma = 1.405, \sigma = 0.74, a_1 = (\pi/2)^{1/2},$$

$$c_1 = 15(\pi/2)^{1/2}/8.$$

The values for $M, R, \Delta Z_0$, have been chosen after many trials and these values have given better results. We have carried out computations also with $E = 1$, but better agreement between $|CH_1|$ and experimental Stanton number is obtained when E is calculated from the expression given in Section 2.

The computations were done at the Computer Centre of DFVLR, AVA, Göttingen using a computer (Siemens 7.865-II) comparable to an IBM-370/168. A special sub-routine (AUTODBL) was used to obtain better accuracy. AUTODBL performs "Double Precision Arithmetic" for the computer program written in "Single Precision Arithmetic".

To achieve a sufficiently high degree of accuracy, the computer program was written in "Double Precision Arithmetic" and AUTODBL was also used. The iterative process was stopped when the difference between two successive iterates was less than the specified tolerance of 10^{-4}. The number of iterations, in general, was between 8 and 15.

More iterations were required in the case of blowing and for the larger values of the wall to stagnation temperature ratio. The computer time for a complete set of solutions of the first- and second-order boundary-layer equations for one data set is about 15 s.

4. DISCUSSION OF RESULTS

Table 1 details the characteristics of the data sets used to analyse the results.

Table 1

Group of data sets	Effect recorded	Remarks
2, 7, 9	Cone-angle	
1, 2	Mach Number	For a 5° cone
6, 7	Mach Number	For a 10° cone
8, 9	Mach Number	For a 15° cone
	Wall to Stagnation	
3, 5	Temperature-Ratio	For a 10° cone
3, 4	Blowing	For a 10° cone

In Figs. 1–4, we have plotted the functions F, H, U and W representing the first- and second-order radial velocity and temperature distributions in the boundary-layer region. Only those curves have been plotted which can be shown clearly and represent distinctly a particular effect. The numbers in circles indicating the curves correspond to the data sets numbers appearing in the first column of Table 2.

In Figs. 3 and 4, the curves for U and W are drawn showing the effects of displacement thickness and transverse curvature. The effects of slip and temperature jump are too small to be shown graphically.

As mentioned earlier, Table 2 shows (in addition to data sets) the first-order inviscid flow quantities on the cone surface and the value of the perturbation parameter ε corresponding to the data sets.

$F'(0)$ and $H'(0)$ along with the skin-friction and heat-transfer coefficients are recorded in Table 3. The negative sign of the quantity $r^{1/2}CH_1$ means that the direction of heat transfer is from the fluid to the body. For the case of hot wall, represented by data set 5, the direction is reversed, e.g. the heat flows from the body to

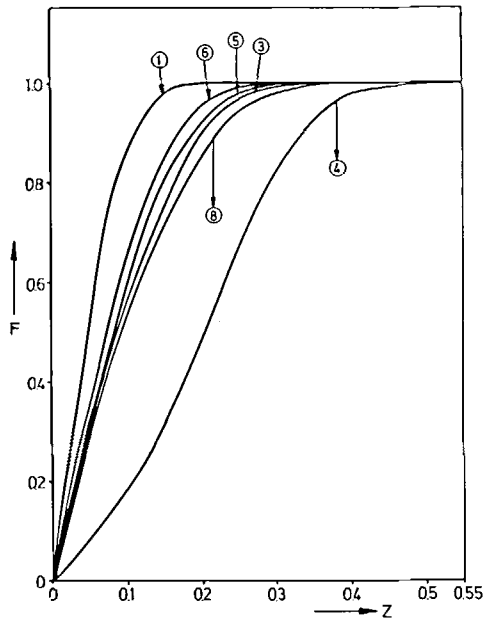

FIG. 1. First-order boundary-layer radial velocity distribution function F.

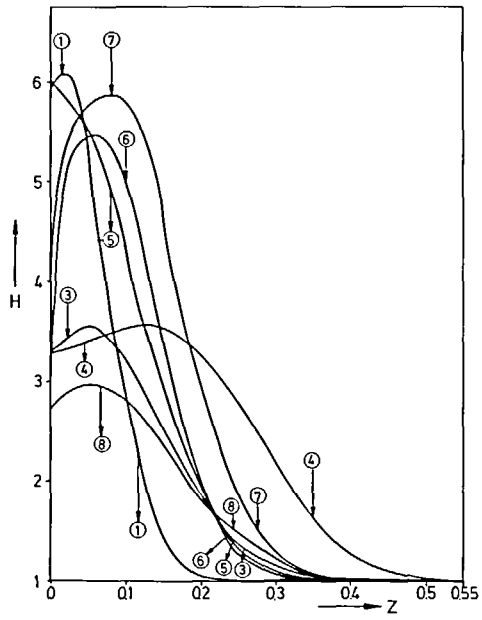

FIG. 2. First-order boundary-layer temperature distribution function H.

the fluid. The absolute value of CH_1 correspond to the local Stanton number.

Table 4 gives the values of $U'(0)$ and $W'(0)$ for each second-order effect.

The quantities CT and CQ, appearing in the expressions for $c_f/\varepsilon c_f^{(1)}$ and $c_Q/\varepsilon c_Q^{(1)}$, respectively, are recorded in Table 5 for each second-order effect.

Table 6 shows the comparison of the absolute values of $r^{1/2}CH_1$ at $r = 1$ and the corresponding experimental value of Stanton number available in various reports at DFVLR, AVA, Göttingen. The agreement between these values is quite good.

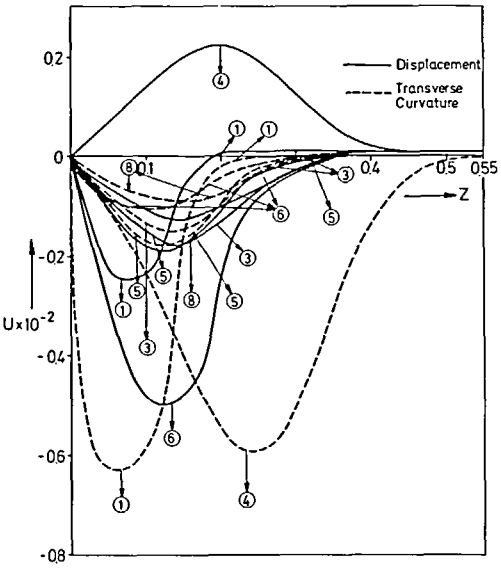

FIG. 3. Second-order boundary-layer radial velocity distribution function U for displacement and transverse curvature effects.

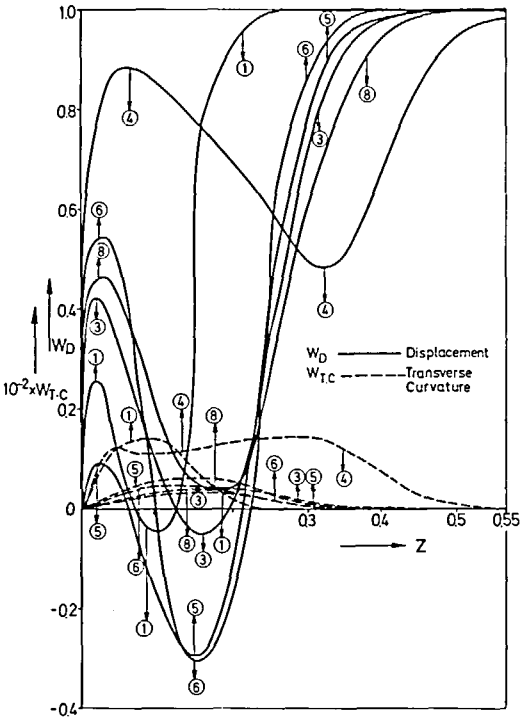

FIG. 4. Second-order boundary-layer temperature distribution function W for displacement and transverse curvature effects.

The conclusions drawn on the basis of these results are given below.

4.1. *First-order boundary-layer flow*

4.1.1. *Effect of cone angle.* We can treat $F'(0)$ as a skin-friction parameter. From Table 3, we observe that $F'(0)$ decreases with increasing cone angle. This amounts to saying that the skin friction decreases with increasing cone angle. Laurmann [22] has found that the drag coefficient c_D increases with decreasing cone angle.

From Table 6, it is clear that for a fixed r, $|CH_1|$ increases with increasing cone angle. Kienappel [23] (Fig. 11, p. 33) has shown graphically that the Stanton number increases with increasing cone angle.

4.1.2. *Effect of Mach number.* Skin friction increases slightly with increasing Mach number. In ref. [22], it is mentioned that there is a small but definite dependence of drag coefficient c_D on free-stream Mach number (M_∞) over the entire range of Reynolds number. Figure 19 on p. 41 of ref. [23] also confirms this. We also note that the magnitude of heat transfer increases with increasing Mach number.

4.1.3. *Effect of wall to stagnation temperature ratio.* Skin friction and the magnitude of the heat transfer increase with increasing value of wall to stagnation temperature ratio. Legge and Dankert [24] have shown that the drag coefficient c_D increases with increasing wall temperature.

4.1.4. *Effect of blowing.* Due to blowing, skin friction, and the magnitude of heat transfer are reduced. Mirels and Ellinwood [25] have given viscous interaction

Table 2. Data sets and the corresponding surface values of inviscid velocity, temperature, pressure along with the values of the perturbation parameter ε

Data set number	Cone semi-vertex angle α	Cone length (cm)	Free-stream Mach number M_∞	Unit Reynolds number UR	Stagnation temperature TS (K)	Wall to stagnation temperature ratio $T_{w1} = T_w/T_s$	Injection parameter $\tilde{V}_w$	First-order inviscid flow velocity on cone U_e	First-order inviscid flow temperature on cone T_e	First-order inviscid pressure on cone P_e	Perturbation parameter ε	Source of data
1	5°	17.15	6.8	1.01×10^5	580	0.68	0	0.989973	0.633746×10^{-1}	0.275587×10^{-1}	0.258716×10^{-2}	[18]
2	5°	7.5	20.8	1510	1560	0.19	0	0.992919	0.127634×10^{-1}	0.166348×10^{-1}	0.904076×10^{-1}	[19]
3	10°	8.5	6.8	7.2×10^4	580	0.52	0	0.965250	0.875441×10^{-1}	0.768841×10^{-1}	0.432756×10^{-2}	[20]
4	10°	8.5	6.8	7.2×10^4	580	0.52	0.5	0.965250	0.875441×10^{-1}	0.768841×10^{-1}	0.432756×10^{-2}	
5	10°	8.39	6.9	3700	300	0.95	0	0.965909	0.873011×10^{-1}	0.810450×10^{-1}	0.238581×10^{-1}	[21]
6	10°	8.5	15.146	3050	1500	0.20	0	0.980385	0.301861×10^{-1}	0.355442×10^{-1}	0.398166×10^{-1}	
7	10°	8.39	20	3050	1450	0.20	0	0.982183	0.277520×10^{-1}	0.494120×10^{-1}	0.584495×10^{-1}	[19]
8	15°	10.4	6.5012	7.2×10^4	580	0.52	0	0.951125	0.106100	0.91355×10^{-1}	0.368806×10^{-2}	
9	15°	5	20	1690	1355	0.22	0	0.961380	0.440470×10^{-1}	0.596087×10^{-1}	0.103599	[19]

Table 3. First-order boundary-layer wall gradients $F'(0)$ and $H'(0)$ of radial velocity and temperature along with the skin-friction and heat-transfer coefficients

Date set number	$F'(0)$	$H'(0)$	$r^{1/2}c_f^{(1)}$	$\varepsilon r^{1/2}c_f^{(1)}$	$r^{1/2}c_Q^{(1)}$	$r^{1/2}CH_1 = \dfrac{\varepsilon r^{1/2}c_Q^{(1)}}{T_0 - T_w}$
1	0.175726×10^1	0.137334×10^1	0.234141	0.605760×10^{-3}	-0.158300×10^{-1}	-0.231267×10^{-3}
2	0.178865×10^1	0.348513×10^2	0.239763	0.216764×10^{-1}	-0.844568×10^{-1}	-0.186404×10^{-1}
3	0.957220	0.168671×10^1	0.371721	0.160865×10^{-2}	-0.802787×10^{-1}	-0.130787×10^{-2}
4	0.227126	0.466494	0.882008×10^{-1}	0.381695×10^{-3}	-0.222028×10^{-1}	-0.361719×10^{-3}
5	0.105164×10^1	−0.750396	0.341332	0.814353×10^{-2}	0.298094×10^{-1}	0.257744×10^{-1}
6	0.114410×10^1	0.104435×10^2	0.328220	0.130686×10^{-1}	−0.124660	-0.121473×10^{-1}
7	0.960305	0.959960×10^1	0.380667	0.222498×10^{-1}	−0.145892	-0.210583×10^{-1}
8	0.868594	0.131857×10^1	0.393403	0.145089×10^{-2}	-0.900262×10^{-1}	-0.123870×10^{-2}
9	0.878752	0.545308×10^1	0.397789	0.412107×10^{-1}	−0.152833	-0.401034×10^{-1}

Table 4. Second-order boundary-layer wall gradients $U'(0)$ and $W'(0)$ of radial velocity and temperature showing the effects of displacement, wall slip, transverse curvature, and temperature jump at the surface

Data set number	$U'(0)$				$W'(0)$			
	Displacement	Transverse curvature	Wall slip	Temperature jump	Displacement	Transverse curvature	Wall slip	Temperature jump
1	-0.887730×10^{2}	-0.240659×10^{3}	-0.119987×10^{1}	-0.531361	0.322205×10^{1}	0.172939×10^{3}	-0.224895×10^{1}	-0.144311×10^{2}
2	-0.400131×10^{3}	-0.826077×10^{2}	-0.889029	-0.705874×10^{1}	0.101261×10^{2}	0.103772×10^{3}	-0.287003×10^{1}	-0.283038×10^{3}
3	-0.302938×10^{2}	-0.252465×10^{2}	-0.150551	-0.107491×10^{1}	0.481967×10^{1}	0.338264×10^{2}	-0.127307×10^{1}	-0.177828×10^{2}
4	-0.195736×10^{2}	-0.260548×10^{2}	0.391021	-0.768919×10^{-1}	0.785526×10^{1}	0.112319×10^{3}	-0.159034×10^{1}	-0.422207×10^{1}
5	-0.375248×10^{2}	-0.332311×10^{2}	-0.214808	0.297441	0.109169×10^{1}	0.418087×10^{2}	-0.156522×10^{1}	-0.489588×10^{1}
6	-0.101440×10^{3}	-0.223110×10^{2}	-0.227942	-0.559160×10^{1}	0.115644×10^{2}	0.381581×10^{2}	-0.194514×10^{1}	-0.137300×10^{3}
7	-0.942648×10^{2}	-0.122610×10^{2}	-0.106084	-0.465962×10^{1}	0.105830×10^{2}	0.260280×10^{2}	-0.168939×10^{1}	-0.980609×10^{2}
8	-0.215396×10^{2}	-0.144587×10^{2}	-0.110464	-0.979549	0.501060×10^{1}	0.194931×10^{2}	-0.106838×10^{1}	-0.148394×10^{2}
9	-0.507640×10^{2}	-0.890342×10^{1}	-0.861353×10^{-1}	-0.381608×10^{1}	0.104991×10^{2}	0.172958×10^{2}	-0.135932×10^{1}	-0.728412×10^{2}

Table 5. Second-order boundary-layer quantities CT and CQ for skin-friction and heat-transfer coefficients showing the effects of displacement, transverse curvature, wall slip, and temperature jump at the surface

Data set number	CT				CQ			
	Displacement	Transverse curvature	Wall slip	Temperature jump	Displacement	Transverse curvature	Wall slip	Temperature jump
1	0.313004×10^{1}	-0.136951×10^{3}	-0.682808	0.571859	0.104620×10^{2}	0.747733×10^{3}	0.421491×10^{2}	-0.606470×10^{2}
2	0.351507×10^{2}	-0.480655×10^{2}	-0.517283	0.111852×10^{2}	-0.128183×10^{1}	0.224154×10^{2}	0.791475×10^{1}	-0.305534×10^{2}
3	0.527343×10^{1}	-0.263748×10^{2}	-0.157280	0.694350	0.592360×10^{2}	0.659220×10^{2}	0.560006×10^{1}	-0.310212×10^{2}
4	0.123101×10^{3}	-0.114715×10^{3}	0.172160×10^{1}	0.164069	0.518823×10^{2}	0.791444×10^{3}	-0.956118×10^{1}	-0.287452×10^{2}
5	0.123878×10^{1}	-0.315994×10^{2}	-0.204260	-0.191442	-0.122057×10^{2}	-0.334588×10^{3}	-0.109702×10^{2}	-0.401295×10^{2}
6	0.217963×10^{2}	-0.195010×10^{2}	-0.199233	0.535772×10^{1}	0.278171	0.123647×10^{2}	0.459858×10^{1}	-0.240005×10^{2}
7	0.214485×10^{2}	-0.127679×10^{2}	-0.110469	0.381175×10^{1}	0.552371	0.989060×10^{1}	0.366172×10^{1}	-0.199350×10^{2}
8	0.478076×10^{1}	-0.166461×10^{2}	-0.127176	0.580030	0.693093×10^{1}	0.404601×10^{2}	0.460739×10^{1}	-0.273852×10^{2}
9	0.150256×10^{2}	-0.101310×10^{2}	-0.980200×10^{1}	0.283086×10^{1}	0.139846×10^{1}	0.801872×10^{1}	0.327000×10^{1}	-0.194237×10^{2}

Table 6. Comparison of the theoretical absolute values of heat-transfer coefficient with the experimental values of Stanton number

Data set number	Absolute value of CH_1 at $r = 1$	Approximate constant minimum value of the experimental Stanton number	Source of the experimental Stanton number	Remarks
1	0.231267×10^{-3}	0.75×10^{-3}	[18], p. 20, Fig. 5	The unit Reynolds number for the experimental result is 1.1×10^5
2	0.186404×10^{-1}	0.015	[19], p. 28, Fig. 9	
3	0.130787×10^{-2}	0.95×10^{-3}	[20], p. 61, Fig. 6	
7	0.210583×10^{-1}	0.023	[19], p. 29, Fig. 10	The unit Reynolds number for the experimental value is 3090
9	0.401034×10^{-1}	0.04	[19], p. 30, Fig. 11	The unit Reynolds number for the experimental value is 1740

theory for slender axisymmetric bodies in hypersonic flow. They have studied weak interaction on a cone and have obtained the result that the drag reduces due to blowing.

4.2. *Second-order boundary-layer flow*

(a) The combined effect of the second-order effects of displacement, transverse curvature, slip and temperature jump results in the decrease in skin friction while the wall pressure increases. Skin friction increases, in general, due to temperature jump while velocity slip reduces skin friction. Individual contribution of each second-order effect on skin friction is recorded in Table 5.

In ref. [25], it is mentioned that the surface slip tends to reduce the magnitude of surface shear.

In ref. [15], it is mentioned that the skin friction coefficient near the stagnation point on a convex wall decreases due to curvature and displacement and the opposite is true for the pressure coefficient at the wall.

(b) From the values of CQ in Table 5 it is clear that the combined effect of wall slip and temperature jump results in the decrease of the rate of heat transfer at the surface. Due to transverse curvature and displacement, the rate of heat transfer is increased in general. In the case of a hot wall, the opposite happens.

Papenfuss [26] has shown that the heat transfer is influenced by the geometry of the surface. Further, the non-continuum effects of wall slip and temperature jump are advantageous with regard to the second-order heat transfer. In ref. [26], higher-order boundary-layer effects at the stagnation point of blunt bodies in laminar hypersonic flow have been studied.

(c) The dominance of second-order effects on skin friction and heat transfer coefficients reduces with increasing cone angle.

(d) The second-order effects become quite significant in the presence of blowing and at high Mach numbers.

(e) From Table 5, it is clear that the transverse curvature and displacement effects have greater significance in comparison to wall slip and temperature jump effects for the flow past cones.

Acknowledgements—The author is grateful to the Alexander von Humboldt Stiftung for the award of a fellowship during 1975–1976 and 1981. He wishes to thank Professor Dr Walter Wuest for many useful discussions and for providing excellent facilities at DFVLR, AVA, Göttingen during the above mentioned period.

REFERENCES

1. W. Hantzsche and H. Wendt, Die laminare Grenzschicht bei einem mit Überschallgeschwindigkeit angeströmten nicht angestellten Kreiskegel, *J. Deut. Luftfahrtforsch.* 76–77 (1971).
2. N. F. Krasnov, *Aerodynamics of Bodies of Revolution* (edited by D. N. Morris), Ch 2. Elsevier, New York (1970).
3. A. P. Krasil'schikov and V. V. Nosov, Some aerodynamic properties of cones in viscous supersonic flow, *Fluid Mech.—Soviet Res.* 9, 18–24 (1980).
4. M. Van Dyke, Higher-order boundary layer theory, *Rev. Fluid Mech.* 1, 265–292 (1969).
5. M. Van Dyke, Higher approximations in boundary layer

theory, Part 1: General analysis, *J. Fluid Mech.* **14**, 161–177 (1962).
6. M. Van Dyke, Higher approximations in boundary layer theory, Part 2: Application to leading edges, *J. Fluid Mech.* **14**, 481–495 (1962).
7. M. Van Dyke, Second-order compressible boundary layer theory with application to blunt bodies in hypersonic flow, *Progress in Astronautics and Rocketry* (edited by F. R. Riddell), Vol. 7, p. 37. Academic Press, New York (1962).
8. R. F. Probstein and D. Elliott, The transverse curvature effect in compressible axially symmetric laminar boundary layer flow, *J. Aeronaut. Sci.* **23**, 208–224, 236 (1956).
9. C. H. Lewis, E. O. Marchand and H. R. Little, Mass transfer and first-order boundary-layer effects on sharp cone drag (a) Part 1: At supersonic conditions (b) Part 2: At hypersonic conditions, *AIAA Jl* **4**, 1697–1703; **4**, 1954–1960 (1966).
10. Z. Kopal, Tables of supersonic flow around cones, Technical Report No. 1, Dept. of Elect. Engg., MIT (1947).
11. J. L. Sims, Tables of supersonic flow around right circular cones at zero angle of attack, George C. Marshall Space Flight Centre, NASA SP-3004 (1964).
12. R. E. Street, The study of boundary conditions in slip flow aerodynamics, *Rarefied Gas Dynamics* (edited by F. M. Devinne), p. 276. Pergamon Press, New York (1960).
13. K. Gersten, H. D. Papenfuss and J. F. Gross, Second-order boundary-layer flow with hard suction, *AIAA Jl* **15**, 1750–1755 (1977).
14. H. Mitome and M. Yasuhara, Compressible boundary layer along wide-angle conical wall, *Trans. Japan Soc. Aero. Space Sci.* **22**, 31–43 (1979).
15. H. Schlichting, *Boundary Layer Theory* (7th edn.), pp. 340, 198 and 195. McGraw-Hill, New York (1979).
16. F. G. Blottner, Variable grid scheme applied to turbulent boundary layers, *Comp. Meth. Appl. Mech. Engng* **4**, 179–194 (1974).
17. F. G. Blottner, Investigation of some finite-difference techniques for solving the boundary layer equations, *Comp. Meth. Appl. Mech. Engng* **6**, 1–30 (1975).
18. K. Kienappel and K. H. Sauerland, Experimentelle Untersuchung des örtlichen Wärmeübergangs an einem schlanken Kegel bei verschiedenen Anstellwinkeln im Rohrwindkanal der DFVLR-AVA. DFVLR, Aerodynamische Versuchsanstalt IB 063-72 H 07 Blatt Nr. 20, Bild 5 (1972).
19. K. Kienappel and D. Vennemann, Experimentelle Untersuchung des örtlichen Wärmeübergangs an schlanken Kegeln in verdünnter Hyperschallströmung, DFVLR-AVA, Bericht No. 71 A 11, Blatt Nr. 33, Bild 11 (1971).
20. P. Krogmann, Experimentelle Untersuchung über die Strömung an Kegeln im Hyperschallbereich zur Ermittlung des Wärmeübergangs des Umschlages laminar/turbulent, DFVLR, AVA, IB No. 251 75 A 25, Blatt Nr. 61, Bild 6 (1975).
21. G. Koppenwallner, Experimentelle Untersuchung der Kräfte an einfachen Flugkörpern bei verdünnter Hyperschallströmung, AVA-Bericht Nr. 69 A 40, Blatt 31, Tabelle 4 und Blatt 42, Bild 11 (1969).
22. J. A. Laurmann, First collision calculation of cone drag under hypersonic rarefied flow conditions, *Astronautica Acta* **13**, 401–404 (1967).
23. K. Kienappel, Experimentelle Untersuchungen an schlanken Kegeln bei verdünnter Hyperschallströmung, DFVLR, AVA Bericht 71 A 10, Blatt Nr. 33, Bild 11 (1971).
24. H. Legge and C. Dankert, Influence of incomplete accommodation in wind tunnel experiments on heat transfer and drag of sharp cones in the transition regime, *Rarefied Gas Dynamics* (edited by S. Fisher), Vol. 74, p. 964. Progress in Astronautics and Aeronautics (1981).
25. H. Mirels and J. W. Ellinwood, Viscous interaction theory for slender axisymmetric bodies in hypersonic flow, *AIAA Jl* **6**, 2061–2070 (1968).
26. H. D. Papenfuss, Higher-order boundary-layer effects at the stagnation point of blunt bodies in laminar hypersonic flow, Proceedings of the 6th U.S. Air Force and the Federal Republic of Germany Data Exchange Agreement Meeting, 28–30 April (1981); DFVLR, AVA. Report IB 222-81 CP 1, 97–109 (1981).

ECOULEMENT DE SECOND ORDRE A COUCHE LIMITE AUTOUR DE CÔNES EFFILES

Résumé—On étudie en détail des effets de second ordre d'épaisseur de déplacement, de courbure transversale, de glissement pariétal et de saut de température pour un écoulement à couche limite sur des cônes effilés de demi-angle 5°, 10° et 15°. Il existe des solutions affines des équations adimensionnelles de premier et de second ordre, et des solutions numériques des systèmes résultants d'équations différentielles sont obtenus en utilisant une technique de différences finies avec pas variable. Les effets de second ordre sont calculés pour différentes valeurs du nombre de Mach, de température de paroi et de paramètre d'injection. Quelques résultats de premier ordre pour le transfert thermique sont comparés à des résultats expérimentaux obtenus au DFVLR.

GRENZSCHICHTSTRÖMUNGEN ZWEITER ORDNUNG AN SPITZEN KEGELN

Zusammenfassung—Grenzschichteffekte zweiter Ordnung wie Verdrängungsdicke, Querkrümmung, Wandschlupf und Temperatursprung wurden ausführlich für Strömungen an spitzen Kegeln mit einem halben Scheitelwinkel von 5°; 10° und 15° untersucht. Es existieren Ähnlichkeitslösungen der dimensionslosen Grenzschichtgleichungen erster und zweiter Ordnung. Numerische Lösungen der resultierenden Systeme gewöhnlicher Differentialgleichungen wurden nach der Methode der finiten Differenzen mit variabler Schrittweite erhalten. Die Grenzschichteffekte zweiter Ordnung wurden für verschiedene Werte der Mach-Zahl, der Wandtemperatur und des Injektionsparameters berechnet. Einige Ergebnisse erster Ordnung für den Wärmeübergangskoeffizienten an der Wand wurden mit bei der DFVLR verfügbaren experimentellen Daten verglichen.

ТЕЧЕНИЕ В ПОГРАНИЧНОМ СЛОЕ У ОСТРЫХ КОНУСОВ, РАССЧИТАННОЕ С УЧЕТОМ ЧЛЕНОВ ВТОРОГО ПОРЯДКА

Аннотация—Проведено детальное исследование влияния учета членов второго порядка на характеристики пограничного слоя – толщину вытеснения, параметр поперечной кривизны, скольжение на стенке и скачок температуры – при обтекании острых конусов с углами полураствора 5°, 10° и 15°. В настоящее время безразмерные уравнения для пограничного слоя, рассчитываемого с учетом первого и второго порядка, решаются автомодельными методами. В работе получены численные решения систем обычных дифференциальных уравнений методом конечных разностей с переменным размером шага. Эффекты второго порядка рассчитываются для различных значений числа Маха, температур стенки и параметров вдува. Проведено сравнение некоторых результатов первого порядка по теплообмену стенки с имеющимися экспериментальными данными.